Fundamental causes of model inaccuracies in predicting wind-blown sand fluxes

Marcelo Chamecki[1] and Jasper F. Kok[2]

[1]University of California, Los Angeles
[2]Department of Atmospheric and Oceanic Sciences University of California, Los Angeles

May 24, 2023

Fundamental causes of model inaccuracies in predicting wind-blown sand fluxes

Marcelo Chamecki[1] and Jasper F. Kok[1]

[1]Department of Atmospheric and Oceanic Sciences, University of California, Los Angeles, CA, USA

Key Points:

- Saltation flux is correlated to, and likely determined by, the fluctuating wind velocities
- Turbulent wind momentum flux is only predictive of sand flux on longer time scales when the former is correlated with the wind velocities
- Predictability of sand flux under realistic field conditions is limited by non-stationary flow and evolving/heterogeneous surface conditions

Corresponding author: Marcelo Chamecki, chamecki@ucla.edu

Abstract

The wind-blown flux of sand generates dunes, wind erosion, and mineral dust aerosols. Existing models predict sand flux using the wind friction velocity that characterizes near-surface turbulent momentum fluxes. However, these models struggle to accurately predict sand fluxes. Here we analyze root causes of these model discrepancies using high-frequency field measurements of winds and sand fluxes. We find that friction velocity is only predictive of sand fluxes on long timescales, when it correlates with horizontal wind speed. On shorter timescales, and for non-ideal surface conditions, friction velocity is much less predictive, likely because the near-surface wind momentum budget is dominated by other, less predictable terms. We furthermore find that variability in 30-min averaged sand fluxes at a given friction velocity is not driven by changes in turbulence but by changes in surface conditions, raising a challenge for models. These findings can improve sand flux models and clarify their limitations.

Plain Language Summary

The wind-blown transport of sand on beaches and in deserts creates sand dunes, causes wind erosion, and generates dust storms. Current theoretical models show large discrepancies in comparisons with measurements. We investigate the fundamental reasons for these discrepancies using high-frequency measurements of sand transport and turbulent winds. We find that the downward transport of horizontal fluid momentum, which models use to predict the wind-blown sand flux, is only predictive when it correlates strongly with the horizontal wind speed itself. This occurs for long (∼30 mins) averaging timescales and idealized surface conditions. But for shorter timescales and realistic field conditions, other processes impact momentum fluxes. These processes are difficult to predict and are not accounted for in current models. Moreover, changes in surface conditions can also drive variability that models do not account for. Our findings help clarify the limitations of existing sand transport models and inform how future models can be improved.

1 Introduction

Wind-blown sand, also known as saltation, shapes the surfaces of Earth and other planets by producing sand dunes and wind erosion (Greeley & Iversen, 1987; Shao, 2008; Kok et al., 2012). Wind-blown sand also drives the emission of mineral dust aerosols, which account for the majority of particulate matter mass in Earth's atmosphere and produce important impacts on climate and human health (Gliß et al., 2021; Kok et al., 2023). But despite the importance of wind-blown sand, the discrepancies of predictive models of sand fluxes (Bagnold, 1941; Owen, 1964; Creyssels et al., 2009) with measurements can be of an order of magnitude (Sherman et al., 2013; Martin & Kok, 2017).

The sand flux depends on the wind momentum flux consumed by wind-blown particles. Most models thus predict the time-averaged sand flux $\overline{q}$ as the product of the wind momentum flux consumed by wind-blown particles τ_p ($\mathrm{N\,m^{-2}}$), multiplied by the efficiency ϵ_p (s) with which this consumption of wind momentum flux is converted into sand flux (Bagnold, 1941; Owen, 1964; Creyssels et al., 2009; Durán et al., 2011; Martin & Kok, 2017). That is,

$$\overline{q} = \epsilon_p \tau_p. \tag{1}$$

A key assumption made by models is that the particle shear stress (τ_p) is entirely supplied by the flux of horizontal momentum transported downward through the fluid by turbulent mixing (τ). This assumption is justified when the flow is stationary and homogeneous, which is the case for canonical boundary layer flow over perfectly flat terrain, averaged over long (e.g., 30 minutes) time periods (Kaimal & Finnigan, 1994;

Van Boxel et al., 2004). This key assumption yields:

$$\tau_p = \tau - \tau_{\mathrm{sfc}}, \tag{2}$$

with

$$\tau = \rho u_*^2 \quad \text{and} \quad \tau_{\mathrm{sfc}} = \rho u_{*,t}^2, \tag{3}$$

where ρ is air density, u_* is wind friction velocity, $u_{*,t}$ is the threshold friction velocity below which saltation cannot be supported, known as the impact or dynamic threshold (Bagnold, 1941), and τ_{sfc} is the wind momentum flux consumed through drag at the surface.

Although sand transport models assuming canonical boundary layer flow show good agreement with some wind tunnel experiments (Creyssels et al., 2009), in many conditions of practical interest the surface layer deviates from canonical conditions, and τ is no longer the only relevant source of momentum into the saltation layer (see Supporting Information). As an example, consider a case in which the mean wind velocity is changing in the streamwise (alongwind) direction due to changes in surface roughness (e.g. caused by sparse vegetation (Okin, 2008; Dupont et al., 2014) or artificial roughness elements (Gillies et al., 2018)), or due to small topographic features such as sand dunes (Sauermann et al., 2001). In these cases, mean momentum advection (Stull, 1988; Garratt, 1990) and/or mean changes in pressure-gradient forces (Belcher & Hunt, 1998) can be comparable to (or even larger than) the turbulent wind momentum flux from above, thus playing an important role in determining the saltation flux.

A related problem is the prediction of saltation fluxes on shorter time scales. The Reynolds equations for the mean flow are typically derived for ensemble averages, and their interpretation in terms of time averages requires stationarity of the turbulence and an averaging time much longer than the integral time scales of turbulence (Lumley & Panofsky, 1964; Lenschow et al., 1994; Salesky & Chamecki, 2012; Wyngaard, 2010). This requirement is discussed in detail in the Supporting Information. Thus, for shorter averaging times (typically less than about 1 or 2 minutes), the assumption that τ represents the main source of momentum is also violated. For such short averaging periods, most terms in the mean momentum budget can be important.

Here we investigate the root causes of why canonical sand transport models show substantial discrepancies with measurements by analyzing high-frequency field measurements of winds and wind-blown sand fluxes. We find that sand transport models (Eqs. 1–3) break down on short timescales because other momentum fluxes become important. Moreover, we surprisingly find that current models also break down on longer timescales even for identical turbulence properties, implying that changes in surface properties drive substantial changes in the sand flux efficiency factor ϵ_p, even at the same field site.

2 Field measurements and data processing

A field campaign designed to provide synchronized high-frequency measurements of wind turbulence and saltation was carried out from May 15 to June 4, 2015 in Oceano, California, USA. The site is located on a gently sloped sand sheet approximately 650 m from the Pacific Ocean. The prevailing wind direction is from the west due to the strong sea breeze during daytime, and the only upwind obstruction consists of fairly small sand dunes located more than 300 m upwind.

The experiment consisted of a vertical array of six sonic anemometers located above a vertical array of nine Wenglor optical particle counters. The sonic anemometers were placed at heights of 0.64, 1.16, 2.07, 3.05, 6.00, and 8.95 m (denoted $S1$

through $S6$), sampling the three components of wind velocity and virtual temperature at a frequency of 50 Hz. The particle counters sampled at 25 Hz were placed between 0.06 and 0.47 m above the surface. BSNE sand traps mounted on wind vanes were used to calibrate horizontal sand fluxes. A more detailed description of the measurements can be found in Martin et al. (2018a). Data from all particle counters were used to produce a time series of vertically integrated horizontal sand flux using the weighted-sum method (Martin et al., 2018a).

The high frequency time series of turbulence and saltation mass flux (Martin et al., 2018b) were divided into 30 minute blocks. Averages and standard deviations within each block for a generic variable a are denoted by $\overline{a}$ and a_{rms}, while further ensemble averaging over all blocks is denoted by $\langle\overline{a}\rangle$. We focus our analysis on 4 different variables: the streamwise and vertical velocity components u and w, the saltation flux q, and the momentum flux $u'w' = (u-\overline{u})(w-\overline{w})$. The time average of the latter yields the friction velocity $u_*^2 = -\overline{u'w'}$. To avoid flow distortion by the tower, only data with an azimuth wind direction within $\pm45^{\mathrm{o}}$ were used. Double rotation of the coordinate system was applied to each sonic anemometer to ensure $\overline{v} = \overline{w} = 0$. No control for stationarity was performed. The focus of the present work is on daytime data from 12 selected days of the field campaign, 5 of which were marked by long periods of continuous saltation.

Following Comola et al. (2019), we define η_q as the fraction of time with non-zero flux records within the 30 minute block (i.e. the fraction of points for which $q > 0$). We use η_q to classify the runs as "no saltation" ($\eta_q < 0.05$), intermittent saltation ($0.05 \leq \eta_q < 0.95$), and continuous saltation ($\eta_q \geq 0.95$). This approach yields 98 blocks, of which 25 blocks are continuous saltation and 51 are intermittent saltation.

To estimate the autocorrelation functions and integral time scales, data was high-pass filtered using a Gaussian filter with a 10-minute window. Integral scales were then computed based on the first zero-crossing of the autocorrelation functions (Dias et al., 2004). Spectral and cospectral analyses were performed by dividing the 30 min blocks into sub-blocks prior to application of FFTs, as standard practice in analysis of micrometeorological data (Kaimal & Finnigan, 1994). Our main results use 20 sub-blocks of 1.5 min each. These are complemented by 5 sub-blocks of 6 minutes to estimate the low-frequency components. We also calculate correlations using filtered time series (represented by $\widetilde{a}$) using a top-hat filter (i.e. a moving average) with 25 averaging windows in the interval $1\,\mathrm{s} \leq \Delta \leq 300\,\mathrm{s}$. We determine the level of correlation between $\widetilde{u}$, $\widetilde{q}$, and $\widetilde{u'w'}$ at different time scales.

We use particle and fluid densities $\rho_p = 2650\,\mathrm{kg/m^3}$ and $\rho_f = 1.22\,\mathrm{kg/m^3}$, and a median grain size $d_{50} = 398\,\mu\mathrm{m}$ determined from grain size distributions (Martin et al., 2018a). The impact threshold friction velocity is estimated to be $u_{*,it} = 0.277\,\mathrm{m/s}$ (Martin & Kok, 2017) and the mean saltation layer height during the observations was $z_q = 0.055\,\mathrm{m}$ (Martin et al., 2018a), so that the lowest sonic anemometer is far from the saltation layer ($z_1/z_q \approx 12$). Assuming ballistic trajectories we obtained a rough estimate of the hopping time for individual grains $t_{\mathrm{hop}} \approx (8z_q/g)^{1/2} \approx 0.2\,\mathrm{s}$ (Martin & Kok, 2017), which is 5 times smaller than the particle inertial response time scale $\tau_p \approx 1\,\mathrm{s}$ (Clift et al., 2005).

3 Results and Discussion

3.1 Data characterization and integral time scales

The current theoretical understanding for splash-dominated equilibrium saltation yields a linear relationship between the mean saltation flux and the excess shear stress at the surface (Creyssels et al., 2009; Martin & Kok, 2017):

$$Q^* = \alpha\left(\Theta - \Theta_c\right). \tag{4}$$

Here, $Q^* = \overline{q}/(\rho_p d\sqrt{gd})$ is the normalized mean saltation flux, $\Theta = u_*^2/(\rho_p gd/\rho_f)$ is the Shields number (Shields, 1936), and Θ_c is a critical Shields number to sustain saltation. Results from our field observations (Fig. 1a) are in reasonable agreement with wind tunnel data (Iversen & Rasmussen, 1999; Creyssels et al., 2009; Ho et al., 2011) when displayed according to Eq. (4). This agreement is supported by the two almost identical fits obtained independently by Creyssels et al. (2009) for wind tunnel data and Martin and Kok (2017) for field data. Overall, this result serves as a confirmation of the linear scaling (1) and that the relationship is approximately the same in the field and in the lab (i.e., it does not seem to be affected by scaling issues such as the much larger integral scale in the field).

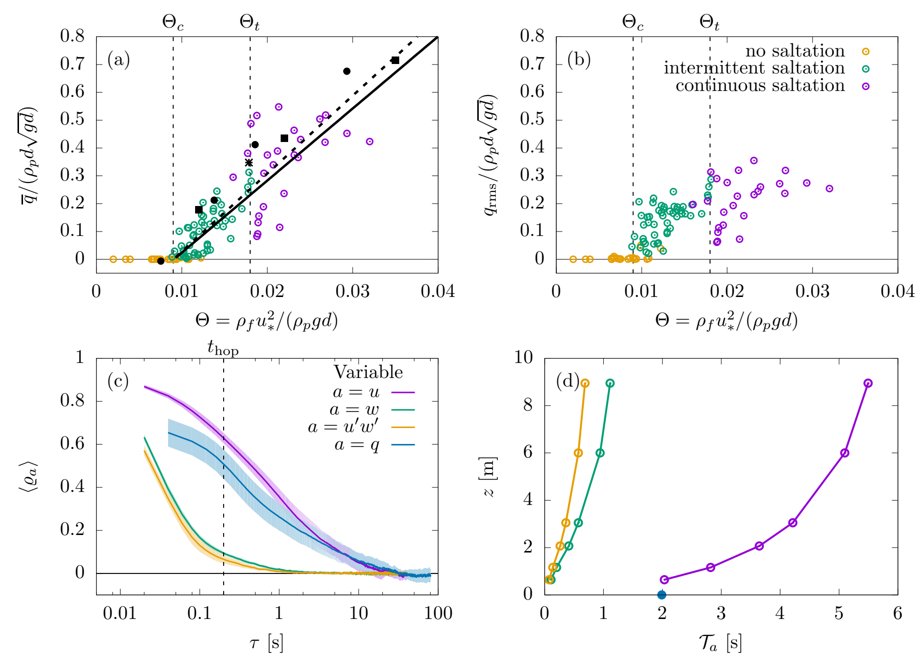

Figure 1. (a) Mean saltation flux and (b) saltation flux variance as a function of Shields number for field observations categorized by saltation regime. Solid and dashed lines indicate fits from Martin and Kok (2017) ($\Theta_c = 0.009$ and $\alpha = 26$) and Creyssels et al. (2009) ($\Theta_c = 0.009$ and $\alpha = 28$), respectively. Black symbols indicate wind tunnel data (squares: Creyssels et al. (2009); circles: Iversen and Rasmussen (1999) and star: Ho et al. (2011)). (c) Ensemble averaged autocorrelation function $\varrho_a(\tau)$ for data at the lowest height and (d) vertical profile of integral scales.

However, as noted by Martin and Kok (2017), there is significant variability in the field data. The correlation coefficient between Q^* and Θ for the field data is equal to 0.45 for continuous saltation and 0.83 if the intermittent saltation regime is also included (see Comola et al., 2019; Li et al., 2020, for model modifications in the intermittent saltation regime). One question to be addressed here is whether this variability can be attributed to differences in the wind forcing (e.g., turbulence properties that are not reflected in the values of u_*) or to changes in surface properties (particle size distribution, moisture content, etc.). Also clear in Fig. 1a is the existence of a transition Shields number (indicated by Θ_t) demarcating the switch from intermittent saltation to continuous saltation (roughly at $\Theta_t \approx 2\Theta_c = 0.018$). The data suggest that the scatter is larger for Shields numbers slightly larger than Θ_t, but there are not enough data to confirm that the scatter reduces for larger values of Θ. Note that there is significant variability in the instantaneous flux within each 30 min period, and that this variability does not have a strong correlation with the Shields number (see Fig. 1b).

Hereafter we focus our analysis on the ensemble of 25 blocks with continuous saltation (magenta circles in Figs. 1a,b). Because our analysis did not show any significant effects of u_* or thermal stability on the results presented below, we only show average results taken over the 25-block ensemble. We characterize the integral scales of the turbulence ($\mathcal{T}$) using autocorrelation functions ($\varrho(\tau)$) (Fig. 1c). Results conform with current understanding of surface layer turbulence: integral scales for u, w, and $u'w'$ increase with increasing height and are much larger for the streamwise velocity than for the vertical velocity or the momentum flux. Note that $\varrho_q(\tau)$ displays a change in behavior around $\tau \approx 0.2\,\mathrm{s}$, which corresponds approximately to the saltation hopping time t_{hop} (this is described below as it is more clearly identified in the spectrum). However, this portion of the curve has almost no effect on the integral scale. The autocorrelation for the saltation flux is very similar to that for the streamwise velocity, a fact that is also reflected by the integral scales shown in Fig. 1d. Note that $\mathcal{T}_q \approx 2\,\mathrm{s}$ is almost identical to $\mathcal{T}_u$ for the lowest sonic, and it is about 10 times larger than the estimated hopping time of individual sand particles. These results are in stark contrast to those obtained by Paterna et al. (2016) for snow saltation in a wind tunnel (see Supplement).

3.2 Spectral analysis

We use spectral and co-spectral analysis to explore the link between streamwise velocity and saltation flux. The frequency spectral density for the streamwise velocity and for the saltation flux conform to traditional surface layer phenomenology, displaying a transition from a f^{-1} scaling in the lower frequencies (i.e., in the production range) to a $f^{-5/3}$ scaling in the inertial subrange (Fig. 2a). Most of the energy in the streamwise velocity is contained at frequencies smaller than τ_p^{-1}, and the peak in the premultiplied spectrum (a proxy for the timescale of the most energetic eddies) is at a frequency $f \approx 0.1\tau_p^{-1}$ (Fig. 2b), confirming that saltating particles should respond quickly to the most energetic eddies.

The spectrum for q departs markedly from the inertial subrange behavior starting at $f \approx 3\,\mathrm{Hz}$.This is clear in the premultiplied spectra shown in Fig. 2b. We cannot explain the large excess in energy at the higher frequencies, and it is possible that this is the result of measurement noise. Hereafter, we only discuss the saltation data up to 2.5Hz to avoid this effect. Most of the analyses are carried out with the 1.5-min blocks for improved convergence, but we rely on 6-min blocks to extend our analysis to lower frequencies (see Fig. 2b). The saltation spectrum has a shape that is typical of other turbulent variables, with one single well defined peak (at $f \approx 0.5\,\mathrm{Hz}$ or 2 seconds) and does not show several distinct peaks as observed by Baas (2006).

The relationship between saltation flux and streamwise velocity and momentum flux as a function of frequency can be characterized by the spectral coherence function defined as

$$\gamma^2_{\alpha,\beta}(f) = \frac{|S_{\alpha\beta}(f)|^2}{S_\alpha(f)S_\beta(f)}, \tag{5}$$

where $S_{\alpha\beta}(f)$ is the cross-spectrum between the two time series involved and $S_\alpha(f)$ and $S_\beta(f)$ are their spectral densities (Bendat & Piersol, 1986; Biltoft & Pardyjak, 2009). Note that $\gamma_{\alpha,\beta}(f)$ can be interpreted as a frequency-dependent correlation coefficient between the two time series ($\gamma_{\alpha,\beta}(f)$ is bounded between 0 and 1, indicating

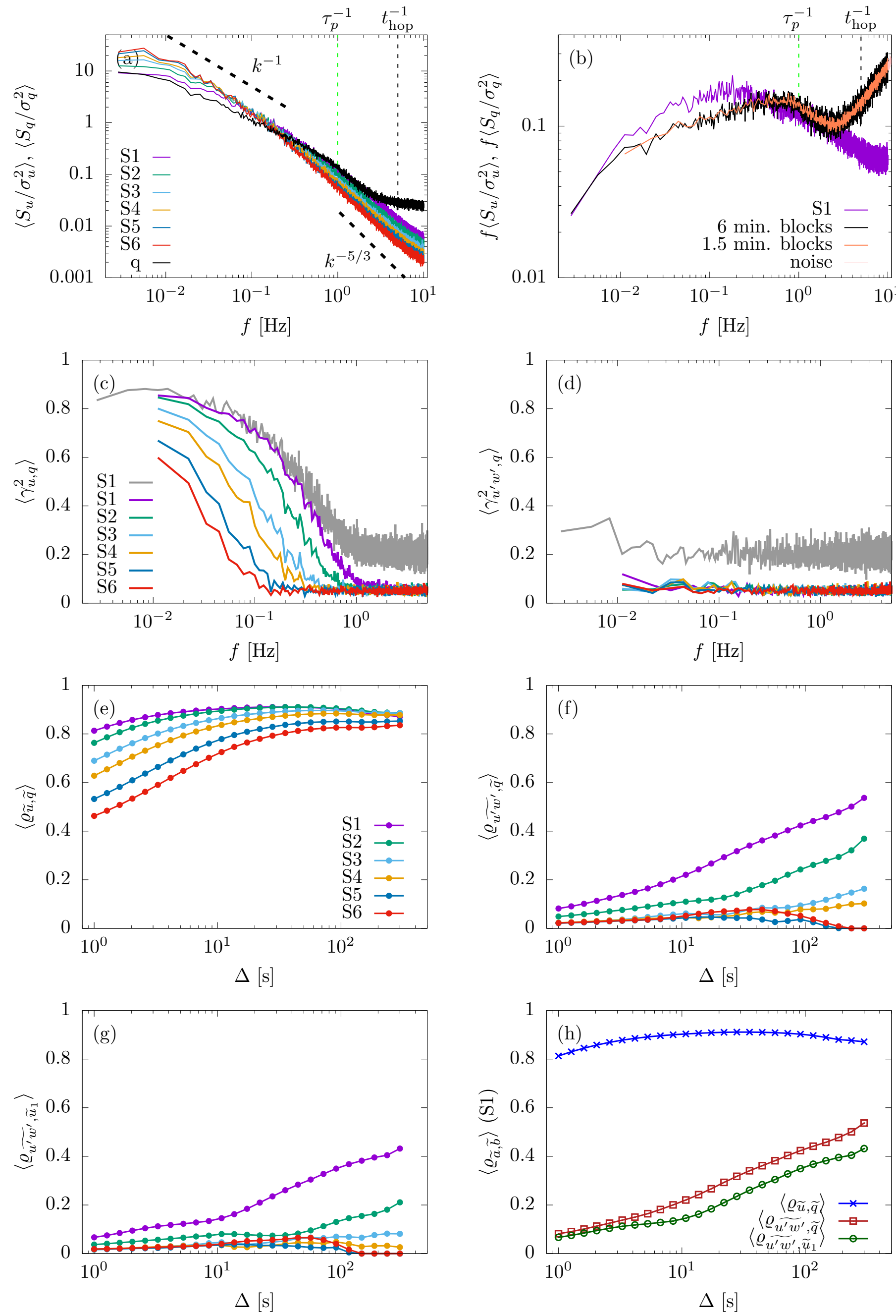

Figure 2. (a) Ensemble averaged spectra for the streamwise velocity and saltation flux. (b) Ensemble averaged spectra for saltation flux and streamwise velocity in premultiplied form. (c) Spectral coherence function between saltation flux and streamwise velocity and (d) between saltation flux and momentum flux. In panels (c) and (d) the grey and colored lines indicate the coherence function obtained from the 6-min and 1.5-min blocks, respectively. Correlation functions between filtered variables as a function of window size Δ: (e) saltation flux and streamwise velocity, (f) saltation flux and turbulent momentum flux, (g) and streamwise velocity and turbulent momentum flux. (h) Correlations using sonic S1 overlaid together.

no correlation and perfect correlation, respectively). The coherence function between streamwise velocity and saltation flux ($\gamma^2_{u,q}$ in Fig. 2c) shows three ranges with distinct behavior: (i) a range in the low frequencies with very strong correlations, (ii) an intermediate range in which the level of correlation decays with increasing frequency, and (iii) a plateau at the noise level in the high frequency range, in which the two time series are uncorrelated. This pattern is especially clear when data from the lowest sonic anemometer (S1) is used. Note the very large coherence below $f \approx 0.1\,\mathrm{Hz}$ for the lowest sonic, which represents the substantial influence of very large-scale motions on these saltation field measurements (Zhang et al., 2023). Extending the frequencies farther in the lower range by using the 6-min. blocks (grey line in Fig. 2c) shows that the large coherence values at the lower end of the spectrum are not an artifact of the analysis procedure. The bias in the high frequency range increases when the number of blocks is reduced. Finally, as the height of the anemometer increases, the intermediate range shifts to lower frequencies, as expected from the increasing spatial separation between the measurements of velocity and saltation. Thus, we interpret the decrease in coherence observed in the intermediate frequency range to be, at least in part, caused by sensor separation (this is true even for the lowest sonic). Therefore, results presented in Fig. 2c suggest a very strong coupling between fluctuations in the saltation flux and the streamwise velocity at all scales in which measurements are not impacted by sensor separation (roughly extending for two decades in the range $2 \times 10^{-3}\,\mathrm{Hz} \leq f \leq 10^{-1}\,\mathrm{Hz}$ for the lowest sonic).

In contrast to the strong correlation between wind speed and saltation flux, $\gamma^2_{u'w',q}$ reveals a complete lack of correlation between saltation flux and momentum flux at any frequency larger than $10^{-2}\,\mathrm{Hz}$ (Fig. 2d). The contrast between $\gamma^2_{u,q}$ and $\gamma^2_{u'w',q}$ strongly indicates that saltation flux is driven by streamwise velocity fluctuations and not by fluctuations in the vertical turbulent momentum flux, at least in the frequency range that can be reliably probed by our analysis ($2\times10^{-3}\,\mathrm{Hz} \leq f \leq 10^{-1}\,\mathrm{Hz}$ corresponding to time scales between 10 seconds and 8 minutes). These results suggest a much simpler picture than the one described by Baas (2006), possibly because the conditions of our field observations are more consistent with canonical surface layers. They also seem to be at odds with the clear relationship between mean saltation flux and mean momentum flux shown in Fig. 1a.

3.3 Effects of averaging time

We investigate this further by calculating correlation coefficients between filtered fields of the 3 main variable of interest: the saltation flux $\widetilde{q}$, the momentum flux $\widetilde{u'w'}$, and the streamwise velocity $\widetilde{u}$. For each filter width Δ, the correlation coefficient obtained reflects the correlation between the two fields considering only the information at scales larger than Δ (the scales smaller than Δ are averaged out by the filter). Note that, by definition, as the filter width Δ approaches 30 min, the filtered fields $\widetilde{q}$, $\widetilde{u'w'}$, and $\widetilde{u}$ converge to their corresponding mean values $\overline{q}$, $\overline{u'w'}$, and $\overline{u}$.

As expected from the behavior of the coherence function in Fig. 2c, reducing Δ causes a decrease in the correlation coefficient between $\widetilde{q}$ and $\widetilde{u}$ (Fig. 2e), as the higher frequencies of q have a weaker correlation with u than the lower frequencies (mostly due to sensor separation). However, this decrease is fairly small, because the lower frequencies contain most of the energy (see Fig. 2a,b) and dominate the behavior of the correlation coefficient. Note also that for large filter widths the correlation coefficient is nearly independent of the sonic height, but the decay in correlation with decreasing Δ starts at larger Δ when u is measured higher up (this is clearly related to the decorrelation caused by spatial separation as discussed above).

Fig. 2f shows the correlation coefficient between saltation flux and momentum flux. While some moderate correlation exists for large filter widths, the correlation decreases quickly with decreasing Δ as higher frequencies are included in the analysis. Note that the momentum flux at heights S3 and above have almost no significant correlation with the saltation flux, in contrast with the large correlations between saltation and streamwise velocity up to the top sonic. More importantly, the increase in the correlation of the saltation flux with the vertical turbulent momentum flux with increasing Δ mirrors the increase in correlation between the momentum flux and the streamwise velocity (Fig. 2g). The similarity between Figs. 2f and 2g is remarkable, and it strongly suggests that the correlation between saltation and momentum flux is indirect and reflects the correlation between momentum flux and streamwise velocity, as hypothesized in Sec. 1. This is seen more clearly when the 3 correlation functions are overlaid together in Fig. 2h (figures for individual saltation days are included in the Supplement). Note that due to estimation constraints, the coherence functions can only be calculated for frequencies down to $f = 2 \times 10^{-3}\,\mathrm{Hz}$ (8 minutes). The correlations in Fig. 2 include all the information on time scales larger than Δ, up to 30 minutes. Thus the moderate correlations between q and $u'w'$ for $\Delta = 300\,\mathrm{s}$ (about 0.5 for sonic S1) suggest that these two quantities are more strongly correlated at time scales longer than 8 minutes than at the sorter time scales captured by the coherence analysis.

3.4 Variability in the 30-min. mean saltation mass flux

To further explore the possible causes of the variability in the relationship between mean saltation mass flux and friction velocity shown in Fig. 1a, the probability distribution function (PDF) for the 3 velocity components, for the momentum flux, and for the saltation mass flux for four selected 30-min blocks are shown in Fig. 3. The blocks have similar friction velocities (corresponding to $\Theta \approx 0.018$) and mean saltation mass fluxes varying by a factor of four. The four blocks have nearly identical PDFs of velocity and momentum flux fluctuations (Fig. 1a-d), as expected for idealized surface layer conditions with similar values of u_*. However the PDFs of instantaneous saltation mass flux are very distinct (Fig. 1e), reflecting the very different mean mass fluxes. Given that the instantaneous mass flux is strongly correlated with the wind velocity fluctuations (this is true for all these four blocks as well), these results eliminate the possibility that the large scatter observed in Fig. 1a can be originated from differences in the turbulence. Therefore, this variability in sand fluxes is likely driven by changes in surface conditions, which can cause especially large variability when wind speeds are near threshold conditions.

4 Conclusions

We have analyzed high-frequency field measurements of winds and wind-blown sand fluxes to investigate the drivers of variability in sand fluxes for similar values of wind friction velocity, and whether those drivers explain why canonical sand transport models show large discrepancies with field measurements. Our results show a strong correlation between the saltation flux and streamwise velocity at all time scales probed, as expected from the mechanistic model for saltation in which the drag imparted to the particles by the wind during their hopping motion is the driver of saltation. Our results also show a lack of correlation between the saltation flux and downward fluid momentum flux for all time scales, except for the long timescales (~30 mins) when the surface layer assumptions of stationarity hold and the momentum flux becomes strongly correlated with the streamwise velocity. We cannot infer cause-and-effect from the correlation coefficients. However, together with the mechanistic model of saltation described in the introduction, results shown in Fig. 2 suggest that the saltation flux is driven by, and thus strongly correlated with, the fluctuations in streamwise velocity. This seems to be true for all the time scales probed here. On the other hand, the

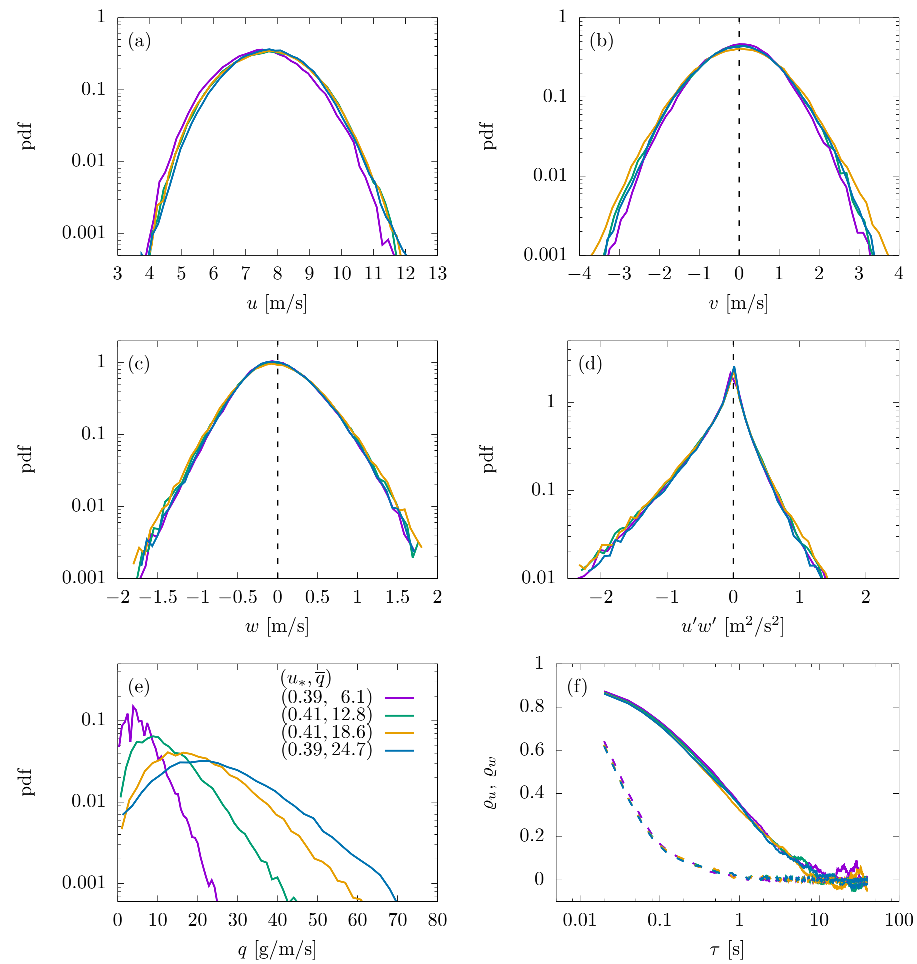

Figure 3. Probability distribution functions (PDFs) for (a) u, (b) v, (c) w, (d) $u'w'$, and (e) q for 4 blocks of continuous saltation with similar values of u_* but very different saltation mass flux $\overline{q}$ (values are indicated in the key). (f) Corresponding autocorrelation functions for u (solid lines) and w (dashed lines).

saltation flux is only correlated to the downward wind momentum flux when the latter is correlated to the streamwise velocity.

These results inform the question of what drives the substantial variability in saltation mass flux on large averaging timescales (∼30 min) that is unexplained by variability in the wind friction velocity u_* (Fig. 1a) (Sherman et al., 2013; Martin & Kok, 2017). The saltation mass flux over a 30-min period is determined by the wind forcing and the surface properties (e.g., Bagnold, 1941). Given the strong correlation between the wind velocity fluctuations and the saltation mass flux at all time scales investigated here (Fig. 2c), we conclude that the bulk of the wind forcing can be characterized by the probability distribution function of the velocity fluctuations. The fact that periods with similar u_* and very different saltation mass fluxes shown in Fig. 1(a) have indistinguishable PDFs of wind fluctuations (see Fig. 3) implies that horizontal heterogeneity did not cause substantial variability in the sand flux at our relatively flat, unvegetated field site (Martin et al., 2018a), although this likely would occur for field sites with less ideal conditions. We conclude that the variability at our field site must be caused by changes in surface properties, including soil size distribution and soil moisture (Wiggs et al., 2004; Martin & Kok, 2019), which can evolve due to erosion exposing surface with different properties. This conclusion is further supported by the fact that most of the variability originates from differences between different days, and not changes that occur within a single day (see Fig. S2 in the Supplement). Finally, the large scatter observed near the threshold Shields number Θ_t in Fig. 1a can be explained by the fact that small changes in surface properties, and thus in Θ_t, can cause large changes in saltation flux for near-threshold conditions.

Our results also inform why canonical saltation models perform poorly on timescales less than 30 minutes (Shao & Mikami, 2005; Martin et al., 2013). At these timescales, the flux of horizontal momentum that is transported downward through the fluid is not necessarily the dominant term in the momentum equation (see Supplement), due to non-stationary flow conditions. This problem can be exacerbated if the terrain is spatially heterogeneous, which could drive additional non-negligible terms in the momentum equation. These issues cause the downward wind momentum flux, and thus u_*, to be only minimally predictive of the streamwise wind speed (Fig. 2g). In turn, this causes poor predictability of the sand flux on short timescales by canonical saltation models that use u_* as the predicting variable.

Our results thus indicate that the predictability of sand fluxes under realistic field conditions is fundamentally limited. On short timescales, the predictability is limited by the violation of the required assumptions of stationarity and horizontal homogeneity in the atmospheric surface layer. These generate non-negligible contributions to the momentum equation, causing large variability in the sand flux at a given value of the friction velocity. On long (∼30-min) timescales, the condition of stationarity is normally satisfied but spatial heterogeneity could still cause substantial variability by generating non-negligible contributions to the momentum equation. Moreover, the longer timescale poses an additional limitation through the variability of surface conditions, such as aeolian transport-induced changes in soil size distribution and topography and weather-induced changes in soil moisture. Overcoming these fundamental limits to the predictability of sand fluxes in realistic field conditions will be difficult, and might require a new theoretical framework, perhaps anchored on the drag forces imparted by the fluctuating winds.

Open Research Section

The data utilized in this paper are available from the Dryad data repository: https://doi.org/10.5061/dryad.rn8pk0p5n.

Acknowledgments

The authors acknowledge funding support from the US National Science Foundation (Grants AGS-1358593 and AGS-1856389), the Cold Regions Research and Engineering Laboratory (Contract No. W913E520C0001), and the U.S. Army Research Laboratory (Grant W911NF2020150). The views and conclusions contained in this document are those of the authors and should not be interpreted as representing the official policies, either expressed or implied, of the Army Research Laboratory or the U.S. Government.

References

Baas, A. C. (2006). Wavelet power spectra of aeolian sand transport by boundary layer turbulence. *Geophysical Research Letters*, *33*(5).

Bagnold, R. (1941). *The physics of blown sand and desert dunes*. Methuen, London.

Batchelor, G. K. (1953). *The theory of homogeneous turbulence*. Cambridge university press.

Belcher, S., & Hunt, J. (1998). Turbulent flow over hills and waves. *Annual Review of Fluid Mechanics*, *30*(1), 507–538.

Bendat, J. S., & Piersol, A. G. (1986). *Random data: analysis and measurement procedures*. John Wiley & Sons.

Biltoft, C. A., & Pardyjak, E. R. (2009). Spectral coherence and the statistical significance of turbulent flux computations. *Journal of atmospheric and oceanic technology*, *26*(2), 403–409.

Chu, C. R., Parlange, M. B., Katul, G. G., & Albertson, J. D. (1996). Probability density functions of turbulent velocity and temperature in the atmospheric surface layer. *Water resources research*, *32*(6), 1681–1688.

Clift, R., Grace, J. R., & Weber, M. E. (2005). Bubbles, drops, and particles.

Comola, F., Kok, J., Chamecki, M., & Martin, R. (2019). The intermittency of wind-driven sand transport. *Geophysical Research Letters*, *46*(22), 13430–13440.

Creyssels, M., Dupont, P., El Moctar, A. O., Valance, A., Cantat, I., Jenkins, J. T., ... Rasmussen, K. R. (2009). Saltating particles in a turbulent boundary layer: experiment and theory. *Journal of Fluid Mechanics*, *625*, 47–74.

Dias, N. L., Chamecki, M., Kan, A., & Okawa, C. M. (2004). A study of spectra, structure and correlation functions and their implications for the stationarity of surface-layer turbulence. *Boundary-layer meteorology*, *110*, 165–189.

Dupont, S., Bergametti, G., & Simoëns, S. (2014). Modeling aeolian erosion in presence of vegetation. *Journal of Geophysical Research: Earth Surface*, *119*(2), 168–187.

Durán, O., Claudin, P., & Andreotti, B. (2011). On aeolian transport: Grain-scale interactions, dynamical mechanisms and scaling laws. *Aeolian Research*, *3*(3), 243–270.

Garratt, J. (1990). The internal boundary layer?a review. *Boundary-layer meteorology*, *50*(1), 171–203.

Gillies, J. A., Etyemezian, V., Nikolich, G., Nickling, W. G., & Kok, J. F. (2018). Changes in the saltation flux following a step-change in macro-roughness. *Earth Surface Processes and Landforms*, *43*(9), 1871–1884.

Gliß, J., Mortier, A., Schulz, M., Andrews, E., Balkanski, Y., Bauer, S. E., ... others (2021). Aerocom phase iii multi-model evaluation of the aerosol life cycle and optical properties using ground-and space-based remote sensing as well as surface in situ observations. *Atmospheric Chemistry and Physics*, *21*(1), 87–128.

Greeley, R., & Iversen, J. D. (1987). *Wind as a geological process: on Earth, Mars, Venus and Titan* (No. 4). CUP Archive.

Ho, T. D., Valance, A., Dupont, P., & El Moctar, A. O. (2011). Scaling laws in aeolian sand transport. *Physical Review Letters*, *106*(9), 094501.

Iversen, J. D., & Rasmussen, K. R. (1999). The effect of wind speed and bed slope on sand transport. *Sedimentology*, *46*(4), 723–731.
Kaimal, J. C., & Finnigan, J. J. (1994). *Atmospheric boundary layer flows: their structure and measurement.* Oxford university press.
Kok, J. F., Parteli, E. J., Michaels, T. I., & Karam, D. B. (2012). The physics of wind-blown sand and dust. *Reports on progress in Physics*, *75*(10), 106901.
Kok, J. F., Storelvmo, T., Karydis, V. A., Adebiyi, A. A., Mahowald, N. M., Evan, A. T., ... Leung, D. M. (2023). Mineral dust aerosol impacts on global climate and climate change. *Nature Reviews Earth & Environment*, *4*, 71–86.
Lenschow, D., Mann, J., & Kristensen, L. (1994). How long is long enough when measuring fluxes and other turbulence statistics? *Journal of Atmospheric and Oceanic Technology*, *11*(3), 661–673.
Li, G., Zhang, J., Herrmann, H., Shao, Y., & Huang, N. (2020). Study of aerodynamic grain entrainment in aeolian transport. *Geophysical Research Letters*, *47*(11), e2019GL086574.
Lumley, J., & Panofsky, H. (1964). *The structure of atmospheric turbulence.* Interscience. (239 pp.)
Martin, R. L., Barchyn, T. E., Hugenholtz, C. H., & Jerolmack, D. J. (2013). Timescale dependence of aeolian sand flux observations under atmospheric turbulence. *Journal of Geophysical Research: Atmospheres*, *118*(16), 9078–9092.
Martin, R. L., & Kok, J. F. (2017). Wind-invariant saltation heights imply linear scaling of aeolian saltation flux with shear stress. *Science Advances*, *3*(6), e1602569.
Martin, R. L., & Kok, J. F. (2019). Size-independent susceptibility to transport in aeolian saltation. *Journal of Geophysical Research: Earth Surface*, *124*(7), 1658–1674.
Martin, R. L., Kok, J. F., Hugenholtz, C. H., Barchyn, T. E., Chamecki, M., & Ellis, J. T. (2018a). High-frequency measurements of aeolian saltation flux: Field-based methodology and applications. *Aeolian Research*, *30*, 97–114.
Martin, R. L., Kok, J. F., Hugenholtz, C. H., Barchyn, T. E., Chamecki, M., & Ellis, J. T. (2018b). *High-frequency measurements of aeolian saltation flux: Time series data [Dataset].* doi: 10.5061/dryad.rn8pk0p5n
Marusic, I., Monty, J. P., Hultmark, M., & Smits, A. J. (2013). On the logarithmic region in wall turbulence. *Journal of Fluid Mechanics*, *716*.
Okin, G. S. (2008). A new model of wind erosion in the presence of vegetation. *Journal of Geophysical Research: Earth Surface*, *113*(F2).
Owen, P. R. (1964). Saltation of uniform grains in air. *Journal of Fluid Mechanics*, *20*(2), 225–242.
Paterna, E., Crivelli, P., & Lehning, M. (2016). Decoupling of mass flux and turbulent wind fluctuations in drifting snow. *Geophysical Research Letters*, *43*(9), 4441–4447.
Perry, A., & Chong, M. (1982). On the mechanism of wall turbulence. *Journal of Fluid Mechanics*, *119*, 173–217.
Salesky, S. T., & Chamecki, M. (2012). Random errors in turbulence measurements in the atmospheric surface layer: implications for monin–obukhov similarity theory. *Journal of the atmospheric sciences*, *69*(12), 3700–3714.
Sauermann, G., Kroy, K., & Herrmann, H. J. (2001). Continuum saltation model for sand dunes. *Physical Review E*, *64*(3), 031305.
Shao, Y. (2008). *Physics and modelling of wind erosion* (Vol. 37). Springer Science & Business Media.
Shao, Y., & Mikami, M. (2005). Heterogeneous saltation: Theory, observation and comparison. *Boundary-layer meteorology*, *115*, 359–379.
Sherman, D. J., Li, B., Ellis, J. T., Farrell, E. J., Maia, L. P., & Granja, H. (2013). Recalibrating aeolian sand transport models. *Earth Surface Processes and*

Landforms, *38*(2), 169–178.
Shields, A. (1936). Application of similarity principles and turbulence research to bed-load movement. *CalTech library*.
Stull, R. B. (1988). *An introduction to boundary layer meteorology* (Vol. 13). Springer Science & Business Media.
Townsend, A. (1976). *The structure of turbulent shear flow.* Cambridge University Press.
Van Boxel, J., Sterk, G., & Arens, S. (2004). Sonic anemometers in aeolian sediment transport research. *Geomorphology*, *59*(1), 131–147.
Wiggs, G., Baird, A., & Atherton, R. (2004). The dynamic effects of moisture on the entrainment and transport of sand by wind. *Geomorphology*, *59*(1-4), 13–30.
Wyngaard, J. C. (2010). *Turbulence in the atmosphere.* Cambridge University Press.
Zhang, X., Zhang, B., Xin, G., & Han, G. (2023). The fluctuating characteristics of streamwise wind speed and total saltation mass flux in the near-neutral atmospheric surface layer. *Physics of Fluids*.